

9, 291 (1967).

<sup>15</sup>J. P. Ostriker and J. E. Gunn, *Astrophys. J.* **157**, 1395 (1969).

<sup>16</sup>J. E. Gunn and J. P. Ostriker, *Phys. Rev. Letters* **22**,

728 (1969).

<sup>17</sup>J. B. Pollack and B. S. P. Shen, *Phys. Rev. Letters* **23**, 1358 (1969).

PHYSICAL REVIEW D

VOLUME 4, NUMBER 1

1 JULY 1971

## Backward-Angle Electron-Proton Elastic Scattering and Proton Electromagnetic Form Factors\*

L. E. Price,† J. R. Dunning, Jr.,‡ M. Goitein,§ K. Hanson, || T. Kirk, and Richard Wilson

*Harvard University, Cambridge, Massachusetts 02138*

(Received 8 February 1971)

Elastic electron-proton scattering cross sections were measured at backward angles ( $80^\circ$ – $90^\circ$ ) in the laboratory for four-momentum transfers between  $7 F^{-2}$  and  $45 F^{-2}$ . Experimental errors range from 3.1% to 5.3%, including a systematic error estimated to be 1.9% added in quadrature. Electric and magnetic form factors are computed from all the recent data in this  $q^2$  range, with allowance made for possible normalization differences. The results show a deviation from the scaling law.

### I. INTRODUCTION

We report here on the second part of a program of measurements of elastic electron-proton scattering, designed to permit form-factor separation. The earlier experiment<sup>1</sup> measured forward-angle scattering. We report now on the measurements of backward angles. The kinematic conditions of our data points are summarized in Table I.

### II. APPARATUS

The apparatus used to scatter the electrons and detect the results is shown schematically in Fig. 1. Electrons from the Cambridge Electron Accelerator (CEA) are directed at a liquid hydrogen target. Electrons scattered at large laboratory angles (usually  $90^\circ$ ) in the horizontal plane enter the spectrometer and are momentum analyzed. The recoiling protons are detected by a scintillation counter telescope. Unscattered electrons continue on to two beam-monitoring devices, a secondary emission monitor (SEM), and a Faraday cup.

The concept of the measurement, and even certain pieces of equipment, were identical with the forward-angle measurement of Ref. 1. We comment here on the differences that were necessary in order to measure backward-angle scattering.

(1) Every effort was made to increase the solid angle of the electron spectrometer as much as possible. Thus a full quadrupole magnet was used in the electron spectrometer instead of the half-quadrupole, used previously. Also the magnet and counters were placed closer to the target.

(2) The electron solid angle was defined in two places. The vertical angle was defined by an aperture  $A_1$  consisting of 0.5 in. of tungsten before the quadrupole. Separate apertures allowed scattered electrons to enter the upper and lower half of the magnet. The horizontal angle was defined after the quadrupole by scintillation counters  $S_L$  and  $S_R$  on either side of a lead aperture 4 in. thick. Each counter overlapped the aperture  $A_2$  by 0.1 in. The fraction of the scattered particles seen by each counter agreed with calculation within the statistical error of 0.1% of the total. For some runs, in fact,  $S_L$  was not working, and it was necessary to rely on the lead aperture  $A_2$  for angular definition on that side.

A Monte Carlo calculation was used to estimate the increase in solid angle from penetration and scattering off the apertures. It was estimated to be  $(0.2 \pm 0.1)\%$ .

Because the angular definition was done in two different places, the solid angle varied with the scattered momentum. At the center of the spectrometer it was 8.4 msr (for the nominal incident beam position).

(3) The array of slat counters  $C_1$ – $C_{16}$ , with edges in the central plane of the quadrupole, which were used to determine the momentum of scattered particles, differed in detail from the one used in Ref. 1. The layout used in this experiment is shown in Fig. 2. The counters were spaced a constant 2 in. apart, giving momentum bins approximately 2% wide. The procedure for determining momentum from the pattern of counter firings is

discussed fully in Ref. 1.

(4) Because the scattered electron energies were lower than for the forward-angle measurement, the 1.0-radiation-length-thick plates, in the lead-Lucite shower counter *S* were replaced by lead plates 0.5 radiation-length thick.

(5) The Čerenkov counter filled with Freon C318 was kept at low pressure (20 in. Hg absolute) in order to reduce the possibility of pions counting by knock-on electrons. In order to count, an electron needed 12 MeV/*c*. Thus pions with momenta below 490 MeV/*c* were prevented from counting by this mechanism. Formerly<sup>1</sup> the gas pressure was high enough that knock-on electrons were counted, though pions could not be counted directly.

(6) The unscattered electron beam was bent slightly by the fringe field of the proton arm sweeping magnet. Thus it was necessary to re-steer the beam, with a small dipole magnet, into the secondary emission monitor (SEM) and Faraday cup.

(7) As in Ref. 1, events were recorded individually by an on-line PDP-1 computer, and the computer trigger was designed to be as loose as possible, serving only to limit the number of uninteresting events accepted. The trigger was

$$E = (1U \text{ OR } 2U) \text{ AND } (15D \text{ OR } 16D) \text{ AND } (S \text{ OR } \check{C}),$$

or the same with up and down interchanged. The minimum signals required from the shower or Čerenkov counter were kept very low. Unwanted events and spurious triggers were eliminated in subsequent analysis of the recorded data.

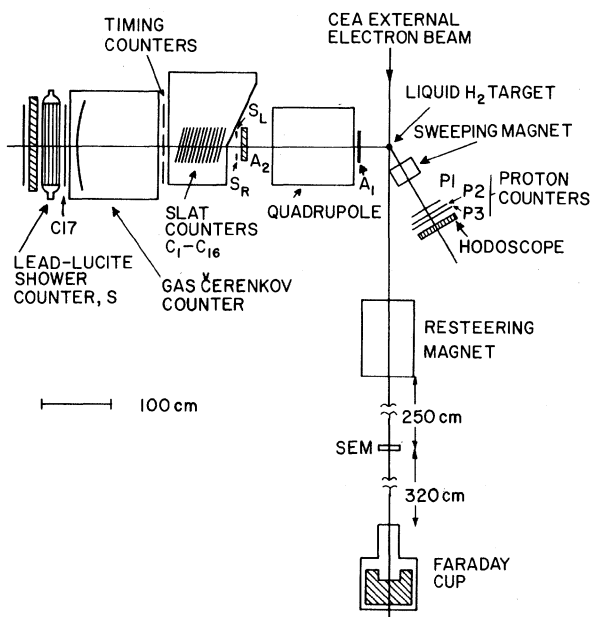


FIG. 1. Schematic layout of experiment.

TABLE I. Kinematic conditions of data points.

$q^2$ ( $F^{-2}$ )	Electron scattering angle (deg)	Incident electron energy (GeV)	Scattered electron energy (GeV)	Recoil- proton angle (deg)
7.00	90.0	0.449	0.304	34.1
10.0	90.0	0.557	0.350	32.1
15.0	90.0	0.718	0.407	29.5
19.7	59.9	1.104	0.696	38.6
20.0	90.0	0.865	0.450	27.5
28.9	90.0	1.104	0.508	24.3
45.0	80.0	1.597	0.664	23.8

In the electron scattering experiments of this group, it is necessary to allow for a dead time, because the monitors (Faraday cup and SEM) cannot be gated off during the computer processing of an event. Under steady operating conditions, this correction is measured directly by comparing with scalars the number of potential triggers to the number accepted by the computer. This measurement normally agrees with that calculated from the trigger rate.

For the first time in this experiment, a problem arose from sudden bursts of "dirty" beam, in which the fraction of random to real potential triggers exceeded the usual by more than an order of magnitude for a short time. At the same time, the potential trigger rate is anomalously large, and most potential triggers are not accepted by the computer. Thus the computer no longer receives a representative sample of the potential triggers, and the losses as measured by the scalars are spuriously large. Cross sections based on this correction are wrong in the extreme case by a factor of 2.

Fortunately, the scaler counting the potential

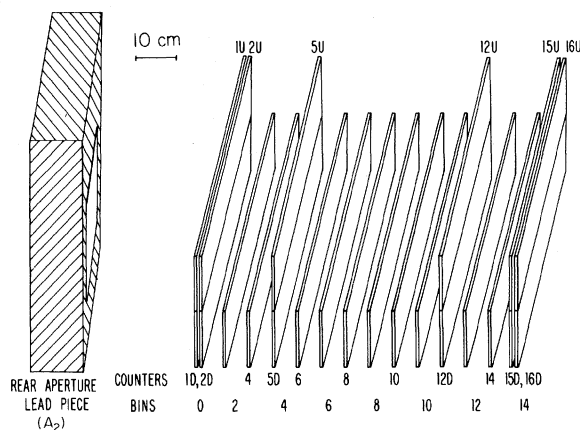


FIG. 2. Momentum-defining slat counters and rear aperture ( $A_2$ ).

triggers was recorded by the computer with each event. Thus these bursts of spurious potential triggers could be identified by detailed analysis. It was found that large bursts of potential triggers were invariably associated with events showing inconsistent tracks in the slat counters on the electron arm. (See Ref. 1 for a description of the analysis of tracks in the slat counters.) So by calculating the dead-time correction from potential triggers associated with events showing good tracks (usually one potential trigger, occasionally two or three), the "dirt" was avoided. This procedure produced agreement with the calculation. Under steady-beam conditions this method also produced agreement with the correction calculated from the scalers. The correction ranged from 0.7% to 4%.

(8) The targets used were of identical design to those used in Ref. 1. The length was about 3.3 cm. An improved method of reducing target boiling was employed which applied heat to the hydrogen returning from the target to the reservoir above. This encouraged more rapid convection, and eliminated all observable bubbling from the target. With no heat, bubbles were observed to form at a rate of about 10/sec.

The pressure in the target was estimated from a gauge on the hydrogen line 50 ft away. Possible differences in pressure lead to an uncertainty in density of 0.25%. The total uncertainty in density and target length is estimated to be  $\pm 0.5\%$ .

(9) Three large scintillation counters 0.5 in. thick were used for the proton telescope. Their size was dictated by the requirements of the companion quasielastic *ed* scattering experiment. For the low- $q^2$  hydrogen measurements, a lead aperture was put before the proton counters to reduce their counting rate. Its size was calculated to allow  $2^\circ$  on all sides beyond the size determined by the mapping of the electron aperture, radiation, and multiple scattering.

### III. ANALYSIS

The purpose of the analysis was to select from all the events sent to the computer those which were due to electron scattering, and, at the same time, to evaluate the efficiencies for the detection. There is sufficient redundancy in the information recorded with every event to permit an unambiguous separation of the desired events from the background and at the same time to measure the efficiencies. This analysis scheme is identical to that used in Ref. 1, where it is described in greater detail.

The detailed procedure was to produce from the data momentum spectra of the scattered electrons

for cuts on other measured quantities, such as Čerenkov or shower pulse heights, or the presence (or absence) of a proton in coincidence.

When the cuts are highly restrictive, with large Čerenkov and shower pulses, and a recoil proton in the right direction, we are confident that the events are almost entirely (99%) due to electron-proton scattering. The momentum spectrum can then be fit to a theoretical distribution, which is the radiative correction calculation (see Sec. VI for details) folded with the calculated spectrometer resolution.

In this fit the momentum focused at the center of the spectrometer is allowed to vary, the normalization is allowed to vary, and it was found necessary to include a variable Gaussian contribution to the spectrometer resolution, representing the sum of a number of small effects not otherwise taken into account.

The fitted theoretical distribution is used to calculate the fraction of the elastic cross section included in our momentum bite, and hence to make the correction for radiation and spectrometer resolution.

### IV. BACKGROUND SUBTRACTION

As in the forward-angle measurement, the kinematic parameters were overdetermined by detecting the recoil proton in the scintillation counters P1, P2, P3, and its direction in the hodoscope. The proton information was instrumental in determining the presence of a background and permitted a correction to be made for it.

First a subtraction was made of the background events which did not show a coincident count in the proton telescope. After subtraction of the empty-target background, the events without a proton in coincidence showed a very broad electron momentum spectrum, corresponding to a slowly varying background with real *ep* scattering events superimposed. (The latter come from those events where the proton was absorbed in one of the proton counters.) The amount of background was estimated by fitting the electron momentum spectrum with no proton present to the form of the spectrum when there was a proton present plus a flat background. After the subtraction the measured proton absorption rate agreed well with calculations. The average absorption over all  $q^2$  points was  $(2.2 \pm 0.2)\%$ , compared with the calculated value  $(3.0 \pm 0.4)\%$ . This gives us confidence in the procedure.

In order to subtract the background that did have a coincident proton, use was made of the proton angular information from the hodoscope. It is expected that events from a source other than elastic electron-proton scattering will not necessarily

give a proton in the small angular region associated by elastic kinematics with the electron's direction. And it is found that events from the tails of the proton angular distribution give broad electron momentum spectra with a strong signal from the slowly varying background. The amount of background with a proton in coincidence was estimated by fitting the electron momentum spectrum and the proton angular distribution to forms associated with good  $ep$  scatters plus flat backgrounds. Only the vertical component of the proton angle was used, because of the small kinematic correlation between the scattered electron momentum and the proton angle in the scattering plane associated with radiation.

The total background subtraction ranged from 5% to 10%, with roughly equal amounts showing a proton in coincidence and showing no proton. We estimate that the uncertainty in the background subtraction introduced by the assumption of flat distributions is no more than 20% of the total subtraction. Thus we have included an error of  $\pm 20\%$  in quadrature with the statistical uncertainties for the subtraction. This constitutes a large portion

of the estimated error on the measurement of the cross section.

The correctness of the subtraction is corroborated by the much improved fits to the momentum spectra that are possible after the data have been cut. Figure 3 shows the momentum spectrum for the  $q^2 = 10 \text{ F}^{-2}$  data in the lower half of the quadrupole for the following cases: (a) All scattered electrons with good shower and Čerenkov pulse heights. The solid line is the computer fit to the data. Its shape depends only on the three peak bins, while the normalization is taken from the whole spectrum. The fit is poor indeed, and shows an excess of observed events in the tails. (b) Proton coincidences only in the hodoscope peak (open points) and in the hodoscope tails (closed points). The solid line is the fit to the hodoscope peak spectrum.

#### V. ORIGIN OF BACKGROUND

The origin of this background is not clear. Charge-symmetric processes like  $\pi^0$  Dalitz decay

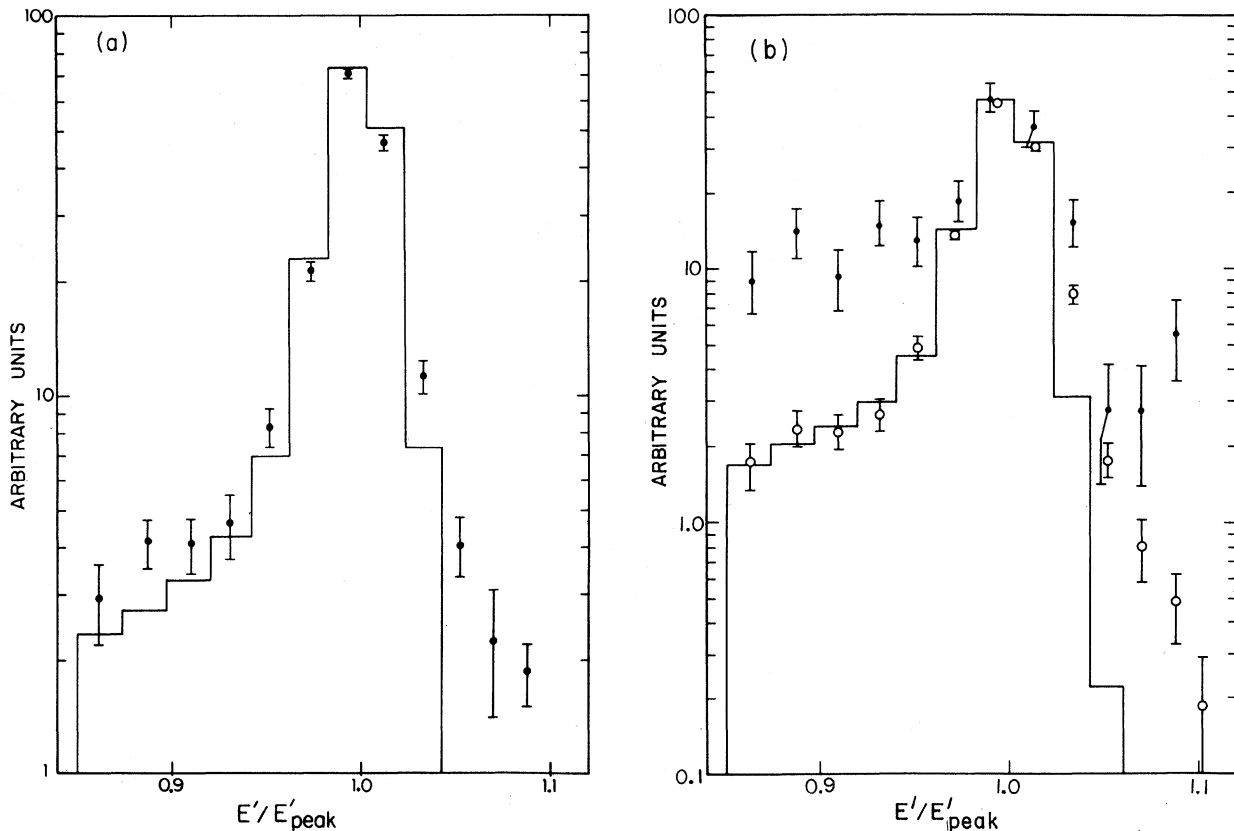


FIG. 3. Momentum spectrum for the  $q^2 = 10 \text{ F}^{-2}$  data in the lower half of the quadrupole for the cases: (a) All scattered electrons with good shower and Čerenkov pulse heights. The solid line is the computer fit to the data. (b) Proton coincidences only in the hodoscope peak (open points) and in the hodoscope tails (closed points). The solid line is the fit to the hodoscope peak spectrum.

are ruled out by runs taken to focus positrons with the quadrupole current reversed. Significant background ( $>1\%$ ) was found this way only for  $q^2 = 45 \text{ F}^{-2}$ , where it amounted to  $(4.6 \pm 1.1)\%$ . Contamination by pions is similarly found to be less than  $1\%$  by the runs taken with a  $\frac{3}{8}$ -in. lead filter blocking the quadrupole aperture. In such a run, most of the electrons (99.8%) are so severely degraded by radiation in the lead that they are unable to pass through the magnet. Pions, on the other hand, are primarily subject only to ionization energy loss and multiple scattering. About 70% are expected to be accepted in the spectrometer's momentum bite with the lead filter in place. A small pion background is correctly handled by our subtraction procedure.

There are small geometric effects that can give correlations between measured electron momentum and proton angle. Thus the electron-proton scattering plane is tipped 0.1 rad from horizontal because the vertical apertures in the magnet are above and below the horizontal plane. Then the change in recoil-proton angle accompanying radiation by the electron before scattering can produce small vertical deviations as well as the horizontal deviations noted earlier. A second effect is produced by multiple scattering into the spectrometer of electrons that would otherwise have missed the aperture, and are thus associated with off-angle protons. In addition, the momentum of these electrons will not, in general, be correctly identified. This second effect is calculated to be small ( $<1\%$ ). It constitutes a background, and our subtraction procedure deals with it correctly. The first effect produces only small angular deviations, and affects mainly the splitting of the peak between the peak angular bins. Thus it does not affect our calculation.

A final possible source of the background which plausibly leads to broadened momentum and proton distributions, as well as to events with no proton in coincidence, is scattering from a heavy nucleus. Since we observe a contribution not subtracted with the empty-target runs, the contaminant must either be mixed with the liquid hydrogen or be deposited on the cold target cup, only to evaporate when the cup is emptied. Analysis of the hydrogen used in one run shows impurities capable of producing, at most, 0.4% of the scattering. Calculations of deposition rates onto the target from residual gas in the scattering chamber, and subsequent observation, suggest an average effect of no more than 1%. In addition, a background from this source would have shown growth with time, which was not observed. Any background from such a source, however, is correctly accounted for by our subtraction procedure.

## VI. NORMALIZATION

The integrated charge from CEA's SEM number 4 and Faraday cup number 2 were monitored to give the number of incident electrons. The Faraday cup gives the number directly without calibration, but was limited at low energies by the loss of a part of the beam from its 9-in. opening through multiple Coulomb scattering. The SEM was closer (see Fig. 1) and larger (12-in. diameter). We were able to calculate the losses (8% in the extreme case) using the Molière theory of multiple scattering.<sup>2</sup> With the corrected Faraday-cup values, the measured SEM efficiency followed within  $\pm 1\%$  the expected Bethe-Bloch energy dependence.<sup>3</sup> At each electron energy, the ratio of charge collected in the SEM to that in the Faraday cup was stable within  $\pm 1\%$ . Thus we have assigned a 1% uncertainty to the beam monitoring.

An additional small ( $\sim 1\%$ ) correction to the incident beam comes from the fraction of electrons so degraded in the target, fluorescent screen, etc. as to bend enough in the corner of the sweeping magnet to miss the restearing magnet.

The solid angle was determined from the measured positions of slits and counters by tracing extreme rays, through the measured<sup>4</sup> field of the quadrupole. Small corrections had to be made for the position of the electron beam, which was determined from fluorescent screens, monitored by television cameras. One was located just downstream of the scattering chamber. Another was mounted directly beneath the target, and could be raised into the beam periodically. Uncertainties in the solid angle come from the ray tracing, from determination of the beam position, and slit penetration (0.2%). The total uncertainty is taken to be 0.6%.

The central scattering angle for the spectrometer was determined by using a transit mounted over the nominal target position to calibrate the angle of the spectrometer relative to the nominal beam line for several standard settings on the protractor at the rear of the spectrometer arm. Subsequently, the arm was set to the desired angle on the protractor. Corrections had to be made for small deviations of the target from its nominal position and of the beam from the nominal beam line. The latter was monitored using the fluorescent screen at the exit of the scattering chamber, and another at the SEM. A small correction ( $0.05^\circ$ ) was introduced by the fringe field of the proton arm sweeping magnet. The scattering angle was determined to  $\pm 0.05^\circ$ , corresponding approximately to  $\pm 0.2\%$  in the cross section.

A new calibration of the CEA energy was undertaken as an adjunct to this experiment. Small de-

viations were found from the former calibration.<sup>5</sup> The maximum error that could have been introduced by using the old calibration was 0.6% in the cross section. It should be noted that the forward angle measurements of Ref. 1 assumed the former calibration. Our interpretation is that the change is due to small movements of the CEA magnets in the intervening time. Corrections amounting to about 1% in the energy had to be made for changing conditions in the accelerator, for electrons arriving before or after the time of peak CEA magnet current, and for ionization loss in the target. We estimate that the average incident energy was known within  $\pm 0.3\%$ .

We have calculated the radiative correction  $\delta$ , starting from the equivalent radiators approximation given by Mo and Tsai.<sup>6</sup> This formula correctly takes account of the variation in matrix element for the scattering process when a photon is radiated from the electron line before scattering. This represents an improvement over the earlier calculations of Tsai<sup>7</sup> and of Meister and Yennie.<sup>8</sup> To this we add the terms from the Meister-Yennie<sup>8</sup> calculation which are constant or proportional to  $Z$  or  $Z^2$ . These are not considered by Mo and Tsai. Finally, we follow the prescription of Yennie, Frautschi, and Suura<sup>9</sup> to exponentiate the doubly

logarithmic terms. Meister and Yennie estimate the uncertainty in the radiative correction as 1.5%. These calculations are similar to those in the forward-angle experiment, and a large part of this uncertainty cancels in a comparison. In addition, we add in quadrature an uncertainty equal to one-quarter of the difference introduced by the matrix element corrections. (In Table II, line 19 gives our calculated correction to the Meister-Yennie radiative correction.)

## VII. CROSS SECTIONS

Table II gives values for the constituents of the cross section for the  $q^2 = 10 \text{ F}^{-2}$  and  $30 \text{ F}^{-2}$  points. The cross section is calculated from these numbers using

$$\frac{d\sigma}{d\Omega} = \frac{N \times \text{correction factors}}{(Q/e)(N_0 \rho l/A) \Delta\Omega},$$

where  $N$  is the number of scattered electrons,  $Q$  is the integrated charge of the incident beam,  $N_0 = 6.023 \times 10^{23}$ ,  $\rho$  is the target density,  $l$  is the length of the target,  $A$  is the atomic weight of hydrogen,  $\Delta\Omega$  is the spectrometer's solid-angle acceptance, and  $e = 1.602 \times 10^{-19} \text{ C}$ .

The cross sections are given in Table III. Quoted errors combine random and systematic

TABLE II. Values and correction factors for cross sections.

	(a) $q^2 = 10 \text{ F}^{-2}$			(b) $q^2 = 28.9 \text{ F}^{-2}$		
	Value	Correction factor	Fractional error (std. dev.)	Value	Correction factor	Fractional error (std. dev.)
1. Number of accepted counts	6327		0.0125	3152		0.0178
2. Empty-target subtraction		0.9770	0.0053		0.9660	0.0077
3. Shower-counter efficiency		1.0816	0.0042		1.2233	0.0121
4. Čerenkov-counter efficiency		1.0101	0.0016		1.1543	0.0098
5. Computer dead time		1.0189	0.0022		1.0105	0.0020
6. Trajectory identification		1.0164	0.0043		1.0190	0.0045
7. Average incident energy (MeV)	522.7	0.9720	0.0109	1094.9	0.9584	0.0152
8. Ionization energy loss		0.9876			0.9858	
9. Average electron scattering angle	89.952	0.9756	0.0025	89.91	0.9950	0.0027
10. Solid angle (msr)	8.331		0.0060	8.323		0.0060
11. Incident charge from Faraday cup or SEM ( $10^{-7} \text{ C}$ )	755.8		0.0100	7700.06		0.0100
12. Beam losses in magnets		0.9913	0.0022		0.9899	0.0025
13. Target length (in. $\text{H}_2$ )	1.322		0.0010	1.322		0.0010
14. Target density ( $\text{g}/\text{cm}^3$ )	0.0708		0.0050	0.0708		0.0050
15. Background subtraction		0.9417	0.0128		0.9065	0.0328
16. Bottom energy accepted (as fraction of elastic energy)	0.8969			0.8987		
17. Top energy accepted (as fraction of elastic energy)	1.0601			1.0623		
18. Radiative correction (Meister)		1.0960	0.0150		1.0982	0.0150
19. Correction for $k$ -dependence of radiation; and resolution		0.9910	0.0023		0.9732	0.0067
Total correction		1.0496	0.0312		1.2663	0.0484

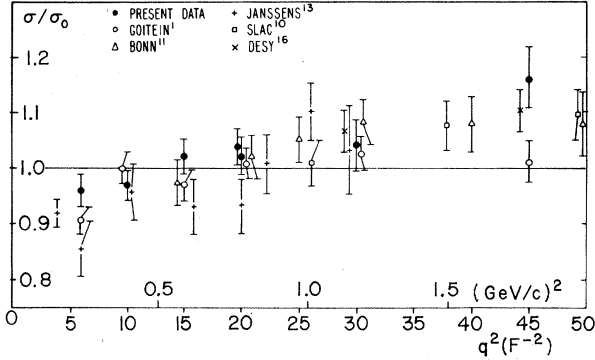


FIG. 4. Ratio of  $ep$  cross sections ( $\sigma$ ) to prediction of dipole ( $\sigma_0$ ) formula and scaling law for the present experiment and other recent data.

uncertainties in quadrature. The systematic contribution is 1.9%. Figure 4 shows these cross sections and selected data from other groups as ratios to the cross sections predicted from the dipole fit to form factors,

$$G_E = (1 + q^2/0.71 \text{ GeV}/c^2)^{-2},$$

and the scaling law.<sup>1</sup> The agreement between groups is seen to be good.

### VIII. FORM-FACTOR FITTING

We have carried out a program of separating proton electromagnetic form factors, combining data from several recent  $ep$  scattering experiments. An attempt was made to correct for possible normalization differences between experiments. We are interested particularly in deviations<sup>11</sup> from the scaling law, which predicts  $\mu_p^2 G_E^2/G_M^2 = 1$ .

The experiments included in the fitting are listed in Table IV. We have excluded data below  $3 \text{ F}^{-2}$  ( $0.116 \text{ GeV}/c^2$ ), and above  $55 \text{ F}^{-2}$  ( $2.14 \text{ GeV}/c^2$ ) from the fitting. Some numbers from these  $q^2$  ranges are quoted in Table V, however, for completeness.

TABLE III. Final cross sections.

$q^2$ ( $\text{F}^{-2}$ )	Angle (deg)	$d\sigma/d\Omega$ ( $10^{-32} \text{ cm}^2/\text{sr}$ )	Fractional error	Ratio to dipole fit
7.00	90.0	2.366	0.031	0.924
7.00	90.0	2.524	0.031	0.986
10.0	90.0	1.202	0.031	0.969
15.0	90.0	0.4872	0.042	1.036
15.0	90.0	0.4806	0.034	1.022
20.0	90.0	0.2156	0.036	1.020
19.7	59.9	0.5957	0.035	1.024
28.9	90.0	0.0702	0.048	1.042
45.0	80.0	0.02032	0.053	1.160

#### A. Normalization

All the data were grouped in bins by  $q^2$  (six intervals between 0 and  $2 \text{ GeV}/c^2$ ) and angle (seven intervals between 0 and  $180^\circ$ ). Within each bin, each cross section was corrected to the value for the central values of  $q^2$  and  $\theta$ , applying the factor that would obtain if the dipole fit correctly described the form factors. The data were then fitted to the hypothesis that all cross sections in a given bin had the same value, using as parameters one normalization factor for each experiment, except that of Goitein *et al.*, which was taken as a reference.

There were 183 data points fitted, in 24 bins that included data from more than one experiment. This leaves 159 degrees of freedom. With all normalization factors set to 1.0, the  $\chi^2$  was 216. When the nine normalization factors were fitted,  $\chi^2$  was reduced to 144. Systematic uncertainties were excluded from the errors used in the least-squares fitting procedure.

The fitted normalization factors are listed in Table IV. They are seen to be consistent with the authors' quoted systematic errors, though no effort was made in the fit to ensure this.

TABLE IV. Normalization factors from fit ( $\sigma_{\text{fit}} = \sigma_{\text{measured}}/N$ ).

Experiment	Reference	$N$	Authors' estimate of normalization error
Goitein <i>et al.</i>	1	...	2.2%
Price <i>et al.</i>	this expt.	$1.011 \pm 0.015$	1.9%
Coward <i>et al.</i>	10	$0.997 \pm 0.012$	4.0%
Berger <i>et al.</i>	11	$0.998 \pm 0.008$	3.5%
Bartel <i>et al.</i>	12	$0.995 \pm 0.011$	3.5%
Janssens <i>et al.</i>	13	$0.987 \pm 0.012$	1.6%
Lehmann <i>et al.</i>	14	$1.017 \pm 0.013$	1.5%
Albrecht <i>et al.</i>	15	$0.979 \pm 0.012$	4.0%
Bartel <i>et al.</i>	16	$0.986 \pm 0.013$	2.4%

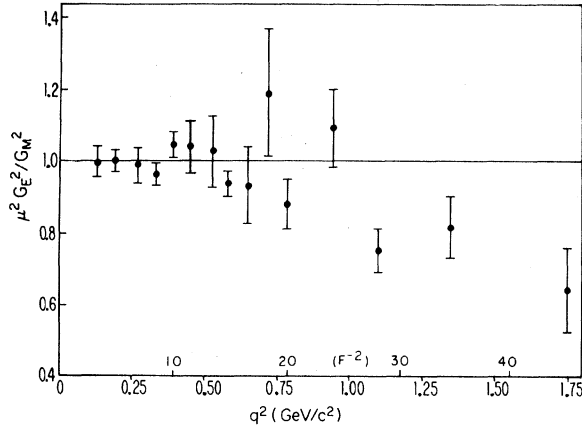


FIG. 5. Fitted ratio  $\mu^2 G_E^2/G_M^2$  versus  $q^2$ . The ratio is seen to deviate from the value of unity predicted by the scaling law.

### B. Form Factors

The data were grouped in bins by  $q^2$ , and all points in a given bin were transformed to a central  $q^2$  value, using the dipole fit and leaving the scattering angle unchanged. The data in each bin were then fitted independently, using as parameters  $G_E^2$  and  $G_M^2$ . A second fitting took as parameters  $G_M^2$  and  $G_E^2/G_M^2$ , in order to get the proper error on the ratio. This procedure involves fewer assumptions about the smooth variation of

the form factors with  $q^2$  than does that of Bilenkaya *et al.*,<sup>17</sup> who fitted the form factors to analytic expressions with a total of five parameters. Table V gives the form factors and the ratio  $\mu^2 G_E^2/G_M^2$  resulting from the fitting. Figure 5 plots this ratio as a function of  $q^2$ .

The results of combining recent cross-section measurements from several groups confirms, with smaller uncertainties, the deviation from the scaling law for  $q^2$  above  $1 \text{ GeV}/c^2$  first reported by the Bonn group.<sup>11</sup> The available data above  $q^2 = 2 \text{ GeV}/c^2$  (see Table V) are not precise enough to confirm a continued deviation.

We note that  $G_E(q^2)/G_M(q^2)$  falls as  $q^2$  increases. We expect therefore that the deviation from the scaling law would be in the opposite direction if the form factors are extrapolated to timelike  $q^2$ . This is the direction needed to meet the threshold condition  $G_E(-4M^2) = G_M(-4M^2)$ , where  $M$  is the proton mass.

### ACKNOWLEDGMENTS

It is a pleasure to thank the engineers, technicians, and crews of the Harvard Cyclotron Laboratory and of the Cambridge Electron Accelerator for their essential contributions in mounting the experiment and in providing the electron beams. L. W. Mo provided valuable advice on making radiative corrections.

TABLE V. Fitted form factors.

$q^2$ (GeV/c <sup>2</sup> )	$G_E^2$	$G_E^2/G_{\text{dipole}}^2$	$G_M^2$	$G_M^2/\mu^2 G_{\text{dipole}}^2$	$\mu^2 G_E^2/G_M^2$
0.0389 <sup>a</sup>	0.776 ± 0.015	0.961	6.296 ± 0.190	1.000	0.961 ± 0.036
0.0778 <sup>a</sup>	0.615 ± 0.018	0.932	4.985 ± 0.151	0.970	0.961 ± 0.042
0.116 <sup>a</sup>	0.526 ± 0.032	0.964	4.141 ± 0.065	0.974	0.990 ± 0.063
0.130	0.481 ± 0.011	0.942	3.76 ± 0.08	0.947	0.994 ± 0.040
0.190	0.367 ± 0.006	0.947	2.861 ± 0.042	0.949	0.998 ± 0.030
0.270	0.253 ± 0.007	0.919	2.002 ± 0.045	0.934	0.984 ± 0.046
0.330	0.1994 ± 0.0044	0.918	1.617 ± 0.021	0.956	0.960 ± 0.032
0.390	0.1716 ± 0.0041	0.989	1.282 ± 0.022	0.949	1.042 ± 0.042
0.450	0.1405 ± 0.0071	1.001	1.053 ± 0.020	0.964	1.038 ± 0.069
0.530	0.1070 ± 0.0074	0.995	1.813 ± 0.026	0.972	1.025 ± 0.100
0.580	(8.67 ± 0.25) × 10 <sup>-2</sup>	0.945	0.719 ± 0.009	1.007	0.939 ± 0.038
0.650	(7.02 ± 0.61) × 10 <sup>-2</sup>	0.946	0.588 ± 0.013	1.017	0.930 ± 0.099
0.720	(7.29 ± 0.93) × 10 <sup>-2</sup>	1.199	0.476 ± 0.014	1.006	1.193 ± 0.181
0.780	(4.71 ± 0.28) × 10 <sup>-2</sup>	0.914	0.418 ± 0.008	1.041	0.878 ± 0.069
0.940	(3.83 ± 0.30) × 10 <sup>-2</sup>	1.118	0.274 ± 0.006	1.027	1.089 ± 0.109
1.100	(1.98 ± 0.14) × 10 <sup>-2</sup>	0.837	0.2046 ± 0.0032	1.110	0.754 ± 0.063
1.350	(1.30 ± 0.12) × 10 <sup>-2</sup>	0.921	0.1241 ± 0.0024	1.130	0.815 ± 0.087
1.750	(0.509 ± 0.091) × 10 <sup>-2</sup>	0.732	(6.17 ± 0.13) × 10 <sup>-2</sup>	1.142	0.642 ± 0.127
2.33 <sup>b</sup>			(2.62 ± 0.12) × 10 <sup>-2</sup>		0.51 ± 0.29
2.50 <sup>c</sup>					1.35 ± 0.44
3.00 <sup>b</sup>			(1.16 ± 0.05) × 10 <sup>-2</sup>		0.40 ± 0.35
3.74 <sup>c</sup>					1.99 ± 0.88

<sup>a</sup>Data from Ref. 14.

<sup>b</sup>Data from Ref. 16.

<sup>c</sup>Data from Ref. 18.

\*Work supported by the U. S. Atomic Energy Commission.

†Presently at Columbia University, New York, N. Y.

‡Presently at California State College at Sonoma, Rohnert Park, Calif.

§Presently at Lawrence Radiation Laboratory, Berkeley, Calif. 94720.

||Presently at Cornell University, Ithaca, N. Y. 14850.

<sup>1</sup>M. Goitein, R. J. Budnitz, L. Carroll, J. R. Chen, J. R. Dunning, Jr., K. Hanson, D. C. Imrie, C. Mistretta, and Richard Wilson, *Phys. Rev. D* **1**, 2449 (1970).

<sup>2</sup>W. T. Scott, *Rev. Mod. Phys.* **35**, 231 (1963).

<sup>3</sup>G. F. Dell and M. Fotino, Cambridge Electron Accelerator Laboratory Report No. CEAL-1045, 1968 (unpublished).

<sup>4</sup>P. F. Cooper (private communication).

<sup>5</sup>H. Winick, Cambridge Electron Accelerator Laboratory Report No. CEAL-1015, 1964 (unpublished).

<sup>6</sup>L. W. Mo and Y. S. Tsai, *Rev. Mod. Phys.* **41**, 205 (1969).

<sup>7</sup>Y. S. Tsai, *Phys. Rev.* **122**, 1898 (1960).

<sup>8</sup>N. Meister and D. R. Yennie, *Phys. Rev.* **130**, 1210 (1963).

<sup>9</sup>D. R. Yennie, S. C. Frautschi, and H. Suura, *Ann. Phys. (N. Y.)* **13**, 379 (1961).

<sup>10</sup>D. H. Coward, H. De Staebler, R. A. Early, J. Litt, A. Minten, L. W. Mo, W. K. H. Panofsky, R. E. Taylor, M. Breidenbach, J. I. Friedman, H. W. Kendall, P. N.

Kirk, B. C. Barish, J. Mar, and J. Pine, *Phys. Rev. Letters* **20**, 292 (1968).

<sup>11</sup>Chr. Berger, E. Gersing, G. Knop, B. Langenbeck, K. Rith, and F. Schumacher, *Phys. Letters* **26B**, 276 (1968); Chr. Berger, V. Burkert, G. Knop, B. Langenbeck, and K. Rith (unpublished).

<sup>12</sup>W. Bartel, B. Dudelzak, H. Krehbiel, J. M. McElroy, U. Meyer-Berkhout, R. J. Morrison, H. Nguyen Ngoc, W. Schmidt, and G. Weber, *Phys. Rev. Letters* **17**, 608 (1966); *Phys. Letters* **25B**, 236 (1967).

<sup>13</sup>T. Janssens, R. Hofstadter, E. B. Hughes, and M. R. Yearian, *Phys. Rev.* **142**, 922 (1966).

<sup>14</sup>P. Lehmann, R. Taylor, and Richard Wilson, *Phys. Rev.* **126**, 1163 (1962); B. Dudelzak, G. Sauvage, and P. Lehmann, *Nuovo Cimento* **28**, 18 (1963).

<sup>15</sup>W. Albrecht, H. J. Behrend, F. W. Brasse, W. Flauger, H. Hultshig, and K. G. Steffen, *Phys. Rev. Letters* **17**, 1192 (1966).

<sup>16</sup>W. Bartel, F.-N. Büsser, W.-R. Dix, R. Felst, D. Harms, H. Krehbiel, P. E. Kuglman, J. McElroy, and G. Weber, *Phys. Letters* **33B**, 245 (1970).

<sup>17</sup>S. I. Bilenkaya, Yu. M. Kazarinov, and L. I. Lapidus, paper submitted to the Fifteenth International Conference on High Energy Physics, Kiev, USSR, 1970 (unpublished).

<sup>18</sup>J. Litt, G. Buschhorn, D. H. Coward, H. DeStaebler, L. W. Mo, R. E. Taylor, B. C. Barish, S. C. Loken, J. Pine, J. I. Friedman, G. C. Hartman, and H. W. Kendall, *Phys. Letters* **31B**, 40 (1970).

PHYSICAL REVIEW D

VOLUME 4, NUMBER 1

1 JULY 1971

## Search for Ionizing Tachyon Pairs From 2.2-GeV/c $K^-p$ Interactions\*

Jerome S. Danburg, George R. Kalbfleisch, Samuel R. Borenstein,†  
Richard C. Strand, and Vance VanderBurg

*Physics Department, Brookhaven National Laboratory, Upton, New York 11973*

and

J. W. Chapman and J. Lys

*Department of Physics, University of Michigan, Ann Arbor, Michigan 48104*

(Received 4 March 1971)

We have searched for pairs of charged particles  $t^+t^-$  with spacelike four-momenta produced in  $K^-p$  interactions at 2.2 GeV/c. It was assumed that such particles could produce visible tracks in the bubble chamber. Under the additional assumption that only tachyons with velocities not much greater than the speed of light ( $v \lesssim 1.7c$ ) could produce visible tracks, the experiment would be sensitive to tachyon invariant masses  $\mu = (-p \cdot p)^{1/2}$  between 100 MeV and 1 GeV and to tachyon-pair invariant-mass-squared values between 0 and 1.44 GeV<sup>2</sup>. No example of the reaction  $K^-p \rightarrow \Lambda t^+t^-$  was found (for momentum transfer squared between 0 and -0.8 GeV<sup>2</sup>), implying a cross section upper limit of  $\approx 0.2 \mu\text{b}$ .

### I. INTRODUCTION

Since the discussion of the possibility of faster-than-light particles in the framework of the special theory of relativity was initiated by Bilaniuk, Deshpande, and Sudarshan<sup>1</sup> in 1962, this topic has attracted considerable theoretical interest. Such

particles would obey the relations

$$E = \frac{\mu}{(v^2 - 1)^{1/2}}, \quad |\vec{p}| = \frac{\mu v}{(v^2 - 1)^{1/2}}$$

and thus

$$E^2 - \vec{p}^2 = -\mu^2 < 0, \quad v = |\vec{p}|/E > 1.$$